

Loophole-free test of local realism via Hardy's violation

Si-Ran Zhao,^{1,2} Shuai Zhao,³ Hai-Hao Dong,^{1,2} Wen-Zhao Liu,^{1,2}
Jing-Ling Chen,⁴ Kai Chen,^{1,2,5} Qiang Zhang,^{1,2,5} and Jian-Wei Pan^{1,2,5}

¹Hefei National Research Center for Physical Sciences at the Microscale and School of Physical Sciences,
University of Science and Technology of China, Hefei, 230026, China

²CAS Center for Excellence in Quantum Information and Quantum Physics,
University of Science and Technology of China, Hefei, 230026, China

³School of Cyberspace, Hangzhou Dianzi University, Hangzhou 310018, China

⁴Theoretical Physics Division, Chern Institute of Mathematics, Nankai University, Tianjin 300071, China

⁵Hefei National Laboratory, University of Science and Technology of China, Hefei, 230026, China

Bell's theorem states that quantum mechanical description on physical quantity cannot be fully explained by local realistic theories, and lays solid basis for various quantum information applications. Hardy's paradox is celebrated to be the simplest form of Bell's theorem concerning its "All versus Nothing" way to test local realism. However, due to experimental imperfections, existing tests of Hardy's paradox require additional assumptions of experimental systems, which constitute potential loopholes for faithfully testing local realistic theories. Here, we experimentally demonstrate Hardy's nonlocality through a photonic entanglement source. By achieving a detection efficiency of 82.2%, a quantum state fidelity of 99.10% and applying high speed quantum random number generators for measurement setting switching, the experiment is implemented in a loophole-free manner. During 6 hours of running, a strong violation of $P_{\text{Hardy}} = 4.646 \times 10^{-4}$ up to 5 standard deviations is observed with 4.32×10^9 trials. A null hypothesis test shows that the results can be explained by local realistic theories with an upper bound probability of 10^{-16348} . These testing results present affirmative evidence against local realism, and provide an advancing benchmark for quantum information applications based on Hardy's paradox.

PACS numbers: 03.65.Ud, 03.67.HK, 03.67.-a

The advent of Quantum Mechanics has exerted a profound impact on our understanding of world. While, it is so counter-intuitive that there exist severe controversies for quantum theory, such as Einstein-Podolsky-Rosen's (EPR's) argument on the completeness of quantum description on physical reality [1]. At the heart of EPR's argument is the paradox between the probabilistic description by quantum theory and the deterministic description by classical theory on physical reality. To explain the probabilistic behavior of quantum theory from classical perspective, Bohm proposed the local hidden variable (LHV) model [2]. Later, Bell presented an inequality as a test whether the quantum behavior can be explained by the LHV model [3, 4]. For quantum theory, the violation of a Bell inequality can be achieved, which indicates that the results from quantum theory cannot be fully explained by the LHV model. This phenomenon is known as Bell nonlocality [5]. The experimental demonstrations of the Bell nonlocality along the routine of Bell inequalities have been conducted soon after its derivation [6, 7], and recently have been pushed into the regime of loophole-free realization [8–13], which promote a vast range of *device-independent (DI) applications* [14–32].

Besides Bell inequalities, there exist other approaches to demonstrate nonlocality, i.e. Bell's theorems without inequality which are emerged since the Greenberger-Horne-Zeilinger (GHZ)'s theorem [5, 33, 34]. The GHZ's theorem pioneers an "All versus Nothing (AVN)" way to test local realism. While, at the very beginning, it's only applicable to three or more-party quantum systems. Soon after, Hardy's paradox is proposed as a "simplest version of Bell's theorem" by simultaneously keeping the "AVN" feature and being applicable to two-

party systems [35, 36]. Specifically, Hardy's paradox is interpreted as that the conditions $P(00|A_2B_2) = 0$, $P(01|A_1B_2) = 0$, $P(10|A_2B_1) = 0$, which must lead to $P(00|A_1B_1) = 0$ for LHV models. While, it can maximally achieve Hardy's value $P(00|A_1B_1) = \frac{5\sqrt{5}-11}{2}$ by quantum theory [35]. Here, $P(ab|xy)$ is the joint probability involving two parties, Alice and Bob, with $x \in \{A_1, A_2\}$ and $y \in \{B_1, B_2\}$ being measurement inputs and $a, b \in \{0, 1\}$ being measurement outputs for Alice and Bob, respectively [5]. Along with this fundamental interest, Hardy's paradox also finds its applications in quantum information processing including DI dimension witness, DI quantum randomness certification, DI quantum key distribution, self-testing of quantum systems and so on [37–42].

Despite great efforts have been made by experimentalists [43–50], loophole-free Hardy's paradox test is still missing, which limits significantly its related quantum information applications. In this letter, we challenge the local realism with Hardy's violation by utilizing polarization-entangled photon pairs with a high-fidelity of up to 99.10%, fast random basis choices, and high detection efficiency of around 82.2% to obtain the joint probabilities of Alice and Bob. Specifically, by simultaneously closing the *locality loophole* and *detection loophole* and using high speed quantum random number generators (QRNGs) to guarantee random measurement setting choices, we demonstrate a Hardy's violation of $P_{\text{Hardy}} = 4.646 \times 10^{-4}$ up to more than 5 standard deviations with a set of events containing 4.32×10^9 trials during 6 hours running time (For local realistic theory, the Hardy's value should be $P_{\text{Hardy}} \leq 0$). By the null hypothesis test following the prediction-based-radio (PBR) method [51], the upper bound of the probability that local realistic theories can repro-

duce the observed Hardy's correlation is $p \leq 10^{-16348}$. These results provide strong evidence that the quantum mechanical predictions cannot be described by local realistic theories. Meanwhile, it serves as a benchmark for quantum information applications based on Hardy's paradoxes.

One of the main obstacles for loophole-free Hardy's paradox test is that, compared with the Bell inequality tests, the theoretical analysis remains incomplete. In practice, due to imperfect detection efficiency $\eta < 1$, there are undetected events, denoted as u . If one discards these undetected events, it will result in a severe *detection loophole*. Here, to test local realism with Hardy's paradox without *detection loophole*, we take these undetected events u into account. During each trial, Alice and Bob choose one of two measurement settings, respectively. The measurement results for Alice and Bob are denoted as ternary elements $a, b \in \{0, 1, u\}$ respectively. Inspired by References [52, 53], when Hardy's conditions $P(00|A_2B_2) = 0$, $P(01|A_1B_2) = 0$ and $P(10|A_2B_1) = 0$ are satisfied, there must be Hardy's value $P_{\text{Hardy}} = P(00|A_1B_1) - P(0u|A_1B_2) - P(u0|A_2B_1) \leq 0$, for local hidden variable models. While, it can achieve positive Hardy's values for quantum theory with

$$P_{\text{Hardy}}^{\max}(\eta) = \frac{1}{2} [1 - \sqrt{1 + 4\eta(3\eta - 2)}] + 3\eta [1 - 3\eta + \sqrt{1 + 4\eta(3\eta - 2)}], \quad (1)$$

for $\eta \in (2/3, 1]$ (See Appendix. A for details).

Besides the imperfect detection efficiency, due to the dark counts of detectors and multiple pairs of photons from the entangled source, there are also some double clicks events in practical experiment, which correspond to the case where both the result 1 and 0 are obtained simultaneously in a single laboratory. Here, in order to close the *detection loophole*, we designate these double clicks events as inconclusive events u , too. Moreover, due to such imperfections, zero Hardy's conditions are experimentally unattainable. Consequently, a form of Hardy's inequality $P_{\text{Hardy}} \leq 0$ together with three Hardy's conditions are necessary for loophole-free Hardy's paradox test. Inspired by the strategy of tackling non-zero Hardy's conditions in References [54, 55], when Hardy's conditions $P(00|A_2B_2) = \epsilon_1$, $P(01|A_1B_2) = \epsilon_2$ and $P(10|A_2B_1) = \epsilon_3$ are satisfied, there must be Hardy's value

$$P_{\text{Hardy}} = P(00|A_1B_1) - P(0u|A_1B_2) - P(u0|A_2B_1) - \sum_{i=1}^3 \epsilon_i \leq 0, \quad (2)$$

for LHV models. Here, u denotes inconclusive events including undetected events and double-click events, ϵ_i with $i \in \{1, 2, 3\}$ are small values for non-zero Hardy's conditions.

Another obstacle is that, compared with the Bell inequality tests, the loophole-free Hardy's paradox test requires even higher detection efficiency and higher fidelity of entangled states. For example, with the system detection efficiency ($\eta \approx 78.8\%$) and quantum state fidelity ($F \approx 98.66\%$) of Reference [11], we show that the Hardy's value should be less

than 10^{-6} , which is quite hard to be realized in a loophole-free manner (See Appendix. A for detail). In the following sections, we experimentally demonstrate a loophole-free Hardy's inequality violation by quantum mechanics statistics as a paradox against local realistic theories.

Experiments.— The present Hardy's paradox test is illustrated in Fig. 1. With the pump laser of 780 nm, the polarization-entangled 1560 nm photon pairs are generated through spontaneous down conversion (SPDC) in the PPKTP crystal within a Sagnac loop. Then the two photons of a pair are transmitted to Alice and Bob's laboratories through fiber links for measurements. To close the *locality loophole* and deal with the *freedom-of-choice loophole* [8–10], we design a space-time configuration for our system, which is shown in Fig. 2. Specifically, it's necessary to space-like separate the setting choices on one side (the first dots on the red bar and blue bar denote the beginning of setting choice) from the measurements output on the other side (the last dots on the two bars denote the ending of the measurement), as well as from the emission of pump photons (the coordinate origin denotes the beginning of the emission of photons and the second dots on the two bars denote the ending of setting choice) which also can be seen as the emission of the hidden variable λ . The synchronization of the experimental system is achieved by locking the seed laser for the pump light, the QRNG for the setting choice and the time-digital convertor (TDC) for the signal collection to the same clock. We carefully adjust the relative delay between the QRNG and pump light to ensure that the polarization of photons could be modulated when the setting choice signal is applied to the Pockels cell at the same time. Meanwhile, the Alice's measurement station is separated far apart from the Bob's measurement station (93 m for Alice from the source to her laboratory, and 90 m for Bob's case), and the length of optical fibers (129 m for Alice and 116 m for Bob) are set appropriately to ensure a time delay of 627 ns and 563 ns respectively from photons' generation to detection.

Furthermore, as for the *freedom-of-choice loophole*, we need to make sure that the random numbers used for measurement setting choices are completely undisturbed and truly random, i.e. the local hidden variables can not manipulate the generation of random numbers. In principle, because that there is an overlap between the backward light cones of two QRNGs and pump laser, the independence and randomness of Alice and Bob's random numbers cannot be proven without making any assumptions [9]. Here, the high speed QRNGs we used could generate random numbers within a time interval of 100 ns after receiving the trigger signal, and the delay time can be flexibly adjusted to accommodate our space-time configuration. A detailed space-time analysis in Fig. 2 shows that *locality loophole* and *freedom-of-choice loophole* can be simultaneously addressed by slightly abusing the assumption on the independence in the generation of random numbers.

The measurements of Alice and Bob consist of Pockels cells, half-wave plates (HWP), polarizing beam splitter (PBS) in turn and finally superconducting nanowire single-photon detectors (SNSPD). To distinguish the result 0, 1, and u experimentally, we place two detectors on two output ports of the

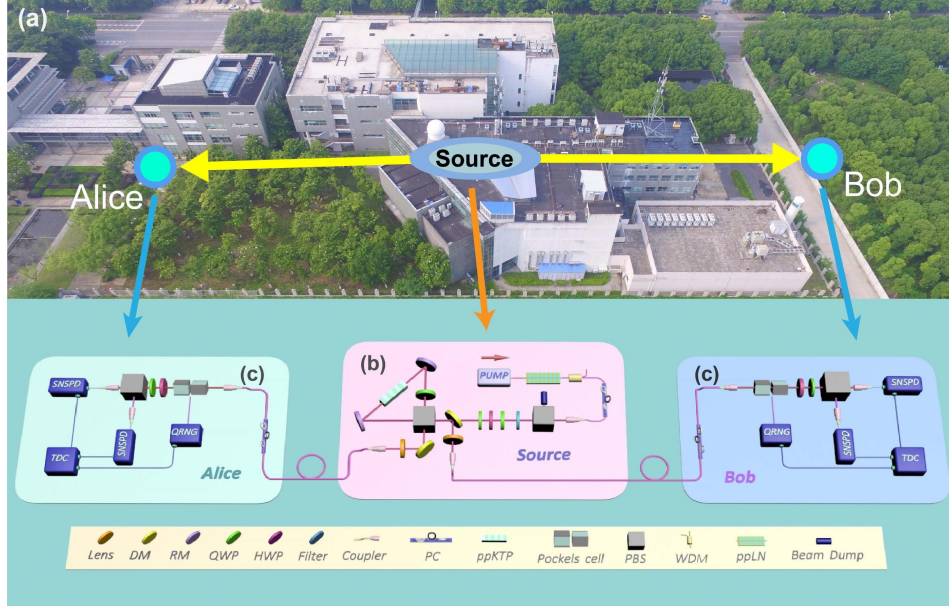


FIG. 1. Schematics of the experiment for loophole-free Hardy's paradox. (a) Bird's-eye view of the experimental apparatus: Alice and Bob are located on opposite sides of the entanglement source, and the straight-line distance between Alice(Bob) and the source is $93 \pm 1(90 \pm 1)$ m. (b) Preparation of entangled photon pairs: Light pulses with a duration of 10 ns and a repetition rate of 200 kHz, generated by a 1560 nm seed laser diode (LD), undergo amplification through an erbium-doped fiber amplifier (EDFA). Subsequently, the pulses are frequency-doubled using an in-line periodically poled lithium niobate (PPLN) crystal. The remaining 1560 nm light is eliminated by a wavelength-division multiplexer (WDM) and spectral filters. Two 780 nm quarter-wave plates (QWPs) and a half-wave plate (HWP) before the Sagnac loop are used to control the polarization of the pump laser thereby changing relative amplitude and phase of the created polarization-entangled photon state. Then the 780 nm pump photons are fed into the periodically poled potassium titanyl phosphate (PPKTP) crystal in the Sagnac loop consist of two reflection mirrors (RMs) and a dual-wavelength polarizing beam splitter (PBS) to generate the polarization-entangled photon pairs of 1560 nm. After the Sagnac loop, we use dichroic mirrors (DM) to remove the residual 780 nm pump laser. Then the entangled photons are collected into optical fibers by coupler and transferred to Alice and Bob in the opposite sites for polarization projection and measurements. (c) Single-photon polarization measurement: At the measurement side, the photons pass through the fiber, and then undergo polarization state measurements. The setup for performing single-photon polarization measurements comprises a Pockels cell, QWP, HWP, and PBS, and are finally collected into a single-mode optical fiber for detection by superconducting nanowire single-photon detectors (SNSPDs). There are two SNSPDs at each side to collect the photons transmitted and reflected at the PBS. The measurement settings choice is performed under a Quantum Random Number Generator (QRNG), which is triggered by a 200 kHz signal and generates a random output with a 1:1 ratio of 0 and 1. Here, 0 corresponds to a low voltage and 1 corresponds to a high voltage. After the random signal is generated, it is applied to the Pockels cell, which modifies the polarization measurement by exerting different influences on polarization at different voltage levels. The time-digital convertor (TDC) is applied to keep track of the photon detection and random number generation events.

PBS and label the clicks on transmission and reflection paths as 0 and 1, respectively. Besides, we denote the undetected events (absence of detector clicks) and double-click events (i.e., clicks on both detectors) at one station as u . The system heralding efficiencies are measured to be $82.1\% \pm 0.2\%$ ($82.4\% \pm 0.2\%$) of transmission (reflection) path for Alice, and $82.1\% \pm 0.2\%$ ($82.2\% \pm 0.2\%$) of transmission (reflection) path for Bob, using the SNSPDs with efficiency higher than 96%. The heralding efficiencies are determined by the ratio of twofold coincidence events to single counts, which corresponds to the total events detected by a single detector directly measured across the entire system without accounting for any losses. These efficiency significantly surpass the record values in previous loophole-free Bell tests with photons (see Table. I). Furthermore, the efficiencies of two paths at each measurement site are adjusted to be close, as any discrepancy in efficiencies can be interpreted as a change of the measurement bases (because this offset affects the ratio of the

probabilities of detecting photons in the transmission and reflection paths). And we employ Hardy's inequality of the form Eq. 2 which has taken all detection events into consideration and inherently closes this loophole.

To observe the Hardy's nonlocality in this experiment, the quantum state $|\psi(\theta)\rangle = \cos(\theta)|HV\rangle + \sin(\theta)|VH\rangle$ and measurement settings $A_i = \cos(\theta_{A_i})\sigma_z + \sin(\theta_{A_i})\sigma_x$, $B_j = \cos(\theta_{B_j})\sigma_z + \sin(\theta_{B_j})\sigma_x$, $i, j \in 1, 2$ are pre-optimized for the overall efficiency $\eta_A(\eta_B)$. Specifically, in the optimization, we set the detection efficiency to be $\eta = 82\%$, the corresponding quantum state, Alice and Bob's measurement settings are optimized to be $\theta = 0.2764$, $\{\theta_{A_1} = -2.8417, \theta_{A_2} = 2.1628\}$ and $\{\theta_{B_1} = 0.2999, \theta_{B_2} = -0.9788\}$ in radian, respectively. (See Appendix. A for details). In the implementation, we measure the visibility to be 99.5% and 98.4% in horizontal/vertical basis and diagonal/antidiagonal basis, respectively. Further, we characterize quantum state by the state tomography measurement, while the fidelity of the non-

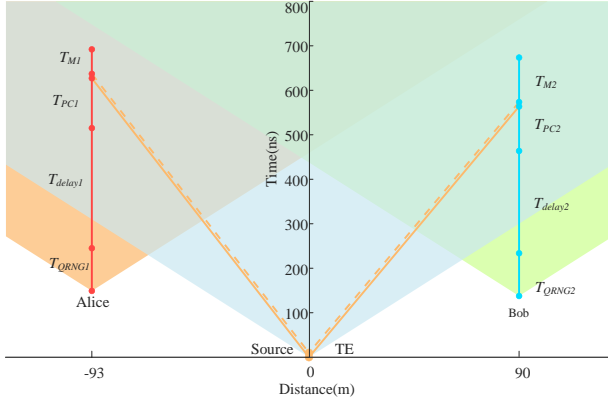


FIG. 2. Space-time diagram for the experimental events. The red (blue) bar and dots represent the crucial time and node for Alice (Bob)'s measurement. The coordinate origin denotes the beginning of the emission of photon pairs. The orange line represents the space-time relationship of photons propagation in the optical fiber (The solid orange line represents the propagation of the photons generated at the onset of the generation, while the dashed orange line represents the photons at the end of the generation). $T_E = 10$ ns is the duration of generating entangled photon pairs. $T_{QRNG1,2}$ are the durations for QRNG to generate random bits to control the Pockels cells. $T_{delay1,2}$ are the times required between the random bits' generation and transferred to Pockels cells. $T_{PC1,2}$ are the preparing time for the Pockels cells to be ready for projection measurements after obtaining random bits from QRNGs. $T_{M1,2}$ are the duration for SNSPDs to output electric signals. $T_{QRNG1} = T_{QRNG2} = 96$ ns, $T_{delay1} = 270$ ns, $T_{delay2} = 230$ ns, $T_{PC1} = 112$ ns, $T_{PC2} = 100$ ns, $T_{M1} = 55$ ns, $T_{M2} = 100$ ns. The linear distance between Alice (Bob) and the source is 93 ± 1 (90 ± 1) m, and the corresponding fiber length is 129 (116) m.

TABLE I. Efficiencies and fidelity in existing photonic experiments of loophole-free Bell tests and related applications. The efficiencies are averaged over Alice's and Bob's detection efficiency.

Label	Experiment	Year	Type	Efficiency	Fidelity
(1)	Shalm <i>et al.</i> [9]	2015	Bell test	75.15%	
(2)	Giustina <i>et al.</i> [10]	2015	Bell test	77.40%	
(3)	Bierhorst <i>et al.</i> [21]	2018	QRNG	75.50%	
(4)	Liu <i>et al.</i> [22]	2018	QRNG	78.65%	
(5)	Li <i>et al.</i> [11]	2018	Bell test	78.75%	98.66%
(6)	Zhang <i>et al.</i> [23]	2020	QRNG	76.00%	
(7)	Shalm <i>et al.</i> [24]	2021	QRNG	76.30%	
(8)	Li <i>et al.</i> [25]	2021	QRNG	81.35%	
(9)	This work	2023	Hardy test	82.22%	99.10%

maximally polarization-entangled state is 99.10% (see See Appendix. B for more details). To reduce the dark count, both the window in which Alice and Bob record detection events is set to 15 ns, which is centered on the expected arrival time of Alice and Bob's photons. The average dark count in this window is less than 5 counts per second. After a stable execution of 6 hours with 4.32×10^9 trials, as shown in Fig. 3, the observed probabilities in the Hardy's paradox test are $\epsilon_1 = P(00|A_2B_2) = (1.120 \pm 0.136) \times 10^{-4}$, $\epsilon_2 = P(01|A_1B_2) = (1.578 \pm 0.162) \times 10^{-4}$,

$\epsilon_3 = P(10|A_2B_1) = (1.818 \pm 0.171) \times 10^{-4}$, $P(0u|A_1B_2) = (1.157 \pm 0.052) \times 10^{-3}$, $P(u0|A_2B_1) = (1.154 \pm 0.056) \times 10^{-3}$, and $P(00|A_1B_1) = (3.227 \pm 0.199) \times 10^{-3}$. These probabilities result in a positive Hardy's value $P_{\text{Hardy}} = 4.646 \times 10^{-4}$ based on the Eq. 2, which is more than 5 standard deviations according to the observed statistics (here the standard deviation is $\sigma = 7.771 \times 10^{-5}$).

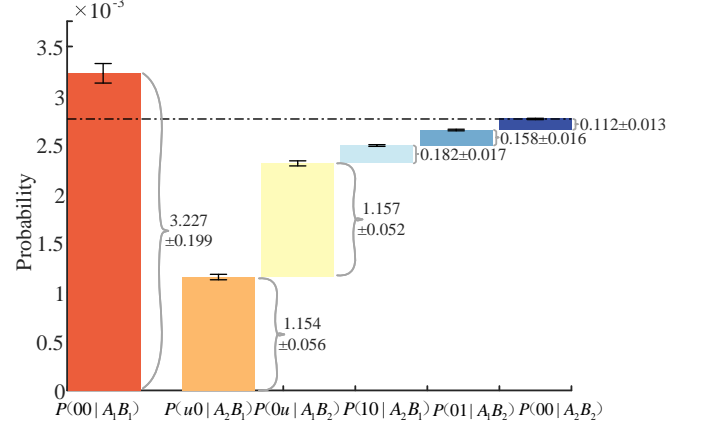


FIG. 3. Bar chart of the six joint probabilities for the present Hardy's paradox. The height of each bar shows the value of the corresponding joint probability. The last three bars represent three Hardy's conditions, which are small quantities relative to the other probabilities. For the height of the first bar representing $P(00|A_1B_1)$ higher than the sum of the other five bars, the P_{Hardy} is positive. These results present strong evidence against local realism

To quantify the statistic significant of the Hardy's violation, we conduct a hypothesis test of local realism with the prediction-based ratio (PBR) method of analysis which allows to analyze the experimental results without assuming independent and identical conditions [51]. The null hypothesis is that the experimental results can be accounted for by local hidden variable models. The maximal probability that the observed experimental results comply with the null hypothesis is quantified by a statistical p value. Under the PBR analysis, our demonstration show that the p value is upper bounded by 10^{-16348} , which is extremely strong evidence against local realism (See Appendix. C for more details).

Discussion and Conclusion.— We have presented a refinement over the theoretical analysis on loophole-free demonstration of Hardy's paradox. By applying high detection efficiency, high fidelity entangled photon source, fast QRNGs, and space-like separating the events corresponding to measurement setting choices, entangled state preparations and photon detections, we have simultaneously closed the *locality loophole*, and addressed the *freedom-of-choice loophole* in the experiment. Combining the strategy of treating double-click events to be inconclusive events and the local hidden variable model under imperfect detection efficiencies, the *detection loophole* is also closed in our experiment at the mean time.

After a stable execution of 6 hours, a positive Hardy's value $P_{\text{Hardy}} = 4.646 \times 10^{-4}$ is observed up to more than 5 standard deviations. Based on a null hypothesis test, the p value that

the possibility our results can be explained by local realistic theories doesn't exceed 10^{-16348} . Therefore, our experiment shows significant evidence that quantum mechanical description on physical quantity cannot be accounted for by local realism. Besides this fundamental interest, these results help to achieve a milestone for quantum information applications based on Hardy's paradox.

Acknowledgments.— S.-R. Z., S. Z. and H.-H. D. contributed equally to this work. This work has been supported by the National Natural Science Foundation of China (Grants No. T2125010, No. 62031024, No. 62375252 and

No. 11875167), the National Key R&D Program of China (Grant No. 2019YFA0308700), the Anhui Initiative in Quantum Information Technologies (Grant No. AHY060200) as well as the Innovation Program for Quantum Science and Technology (Grant No. 2021ZD0301100). J. L. C. was supported by the National Natural Science Foundations of China (Grant Nos. 12275136 and 12075001) and the 111 project of B23045. S. Z. is supported by the Research Startup Foundation of Hangzhou Dianzi University (No. KYS275623071) and Zhejiang Provincial Natural Science Foundation of China under Grant No. LQ24A050005.

Appendix A: Optimal quantum state and measurement settings under imperfect detection efficiency

At the beginning of the experiment, we optimize the quantum state and measurement settings by considering imperfect system detection efficiency $\eta \in [0, 1]$. Following the formalism in the original Hardy's paradox [35], the two-qubit entangled state is modeled as

$$|\Psi(\theta)\rangle = \cos(\theta)|01\rangle + \sin(\theta)|10\rangle, \quad (\text{A1})$$

where $\theta \in [0, \frac{\pi}{2}]$ is an adjustable parameter. When $\theta = \frac{\pi}{4}$, the quantum state becomes a maximal entangled state. For Alice and Bob's binary observables $\{A_1, A_2\}$ and $\{B_1, B_2\}$, corresponding projectors are

$$\begin{aligned} \Pi_{A_i}^a &= |A_i^a\rangle\langle A_i^a|, \\ \Pi_{B_j}^b &= |B_j^b\rangle\langle B_j^b|. \end{aligned} \quad (\text{A2})$$

with $i, j \in \{1, 2\}$ and $a, b \in \{0, 1\}$. Firstly, we take the basis vectors for Alice and Bob's measurements A_2 and B_2 to be

$$\begin{aligned} |A_2^0\rangle &= \beta_2|0\rangle + \alpha_2|1\rangle, \\ |A_2^1\rangle &= \alpha_2|0\rangle - \beta_2|1\rangle, \\ \text{and} \\ |B_2^0\rangle &= -\alpha_2|0\rangle + \beta_2|1\rangle, \\ |B_2^1\rangle &= \beta_2|0\rangle + \alpha_2|1\rangle. \end{aligned} \quad (\text{A3})$$

Without loss of generality, we have taken amplitudes α_2 and β_2 to be real. Then, the state in the Eq. A1 can be rewritten as

$$\begin{aligned} |\Psi(\theta)\rangle &= [\cos(\theta)\beta_2^2 - \sin(\theta)\alpha_2^2]|A_2^0\rangle|B_2^0\rangle + [\cos(\theta)\alpha_2\beta_2 + \sin(\theta)\alpha_2\beta_2]|A_2^0\rangle|B_2^1\rangle \\ &\quad + [\cos(\theta)\alpha_2\beta_2 + \sin(\theta)\alpha_2\beta_2]|A_2^1\rangle|B_2^0\rangle + [\cos(\theta)\alpha_2^2 - \sin(\theta)\beta_2^2]|A_2^1\rangle|B_2^1\rangle. \end{aligned} \quad (\text{A4})$$

By taking the first term of Eq. A4 to be

$$\cos(\theta)\beta_2^2 - \sin(\theta)\alpha_2^2 = 0,$$

we have

$$k^2 \equiv \frac{\alpha_2^2}{\cos(\theta)} = \frac{\beta_2^2}{\sin(\theta)}. \quad (\text{A5})$$

Considering $\alpha_2^2 + \beta_2^2 = 1$, k is taken to be $k = \frac{1}{\sqrt{\cos(\theta) + \sin(\theta)}}$ and $\alpha_2 = k\sqrt{\cos(\theta)}$, $\beta_2 = k\sqrt{\sin(\theta)}$. Thus, the first Hardy condition is satisfied,

$$P(00|A_2B_2) = \text{Tr}(\Pi_{A_2}^0 \otimes \Pi_{B_2}^0 |\Psi\rangle\langle\Psi|) = 0. \quad (\text{A6})$$

Here, the k , α_2 , and β_2 have been taken as positive parameters without loss of generality. Then, the state in the Eq. A4 becomes

$$\begin{aligned} |\Psi(\theta)\rangle &= \sqrt{\sin(\theta)\cos(\theta)}|A_2^0\rangle|B_2^1\rangle + \sqrt{\sin(\theta)\cos(\theta)}|A_2^1\rangle|B_2^0\rangle + [\cos(\theta) - \sin(\theta)]|A_2^1\rangle|B_2^1\rangle \\ &= \left[\frac{\sqrt{\sin(\theta)\cos(\theta)}}{\sqrt{\cos(\theta) - \sin(\theta)}}|A_2^0\rangle + \sqrt{\cos(\theta) - \sin(\theta)}|A_2^1\rangle \right] \cdot \left[\frac{\sqrt{\sin(\theta)\cos(\theta)}}{\sqrt{\cos(\theta) - \sin(\theta)}}|B_2^0\rangle + \sqrt{\cos(\theta) - \sin(\theta)}|B_2^1\rangle \right] \\ &\quad - \frac{\sin(\theta)\cos(\theta)}{\cos(\theta) - \sin(\theta)}|A_2^0\rangle|B_2^0\rangle. \end{aligned} \quad (\text{A7})$$

Now, we choose the observable basis vectors for Alice and Bob's measurements A_1 and B_1 to be

$$\begin{aligned} |A_1^0\rangle &= -\beta_1 |A_2^0\rangle + \alpha_1 |A_2^1\rangle, \\ |A_1^1\rangle &= \alpha_1 |A_2^0\rangle + \beta_1 |A_2^1\rangle, \\ \text{and} \\ |B_1^0\rangle &= -\beta_1 |B_2^0\rangle + \alpha_1 |B_2^1\rangle, \\ |B_1^1\rangle &= \alpha_1 |B_2^0\rangle + \beta_1 |B_2^1\rangle. \end{aligned} \quad (\text{A8})$$

with $\alpha_1 = \frac{\sqrt{\cos(\theta)\sin(\theta)}}{\sqrt{1-\cos(\theta)\sin(\theta)}}$, $\beta_1 = \frac{\cos(\theta)-\sin(\theta)}{\sqrt{1-\cos(\theta)\sin(\theta)}}$ and $N = \frac{1-\cos(\theta)\sin(\theta)}{\cos(\theta)-\sin(\theta)}$. Then, the state in the Eq. A7 becomes

$$|\Psi\rangle = N(|A_1^1\rangle|B_1^1\rangle - \alpha_1^2 |A_2^0\rangle|B_2^0\rangle). \quad (\text{A9})$$

Then, in measurement settings A_2B_2 , A_1B_2 , A_2B_1 and A_1B_1 , respectively, the quantum state can be rewritten as follows

$$|\Psi\rangle = N(\alpha_1\beta_1 |A_2^0\rangle|B_2^1\rangle + \alpha_1\beta_1 |A_2^1\rangle|B_2^0\rangle + \beta_1^2 |A_2^1\rangle|B_2^1\rangle), \quad (\text{A10a})$$

$$|\Psi\rangle = N[|A_1^1\rangle(\alpha_1 |B_2^0\rangle + \beta_1 |B_2^1\rangle) - \alpha_1^2 (-\beta_1 |A_1^0\rangle + \alpha_1 |A_1^1\rangle)|B_2^0\rangle], \quad (\text{A10b})$$

$$|\Psi\rangle = N[(\alpha_1 |A_2^0\rangle + \beta_1 |A_2^1\rangle)|B_1^1\rangle - \alpha_1^2 |A_2^0\rangle(-\beta_1 |B_1^0\rangle + \alpha_1 |B_1^1\rangle)], \quad (\text{A10c})$$

$$|\Psi\rangle = N[|A_1^1\rangle|B_1^1\rangle - \alpha_1^2 (-\beta_1 |A_1^0\rangle + \alpha_1 |A_1^1\rangle)(-\beta_1 |B_1^0\rangle + \alpha_1 |B_1^1\rangle)] \quad (\text{A10d})$$

From the Eq. A10a, Eq. A10b and Eq. A10c, we have $P(00|A_2B_2) = 0$, $P(01|A_1B_2) = 0$, and $P(10|A_2B_1) = 0$, respectively. While, from the Eq. A10d, we have

$$P(00|A_1B_1) = |\langle A_1^0 B_1^0 | \Psi \rangle|^2 = |N\alpha_1^2 \beta_1^2|^2. \quad (\text{A11})$$

The Hardy's value $P(00|A_1B_1)$ can achieve a non-zero value. By considering that $A_i = \Pi_{A_i}^0 - \Pi_{A_i}^1$ and $B_j = \Pi_{B_j}^0 - \Pi_{B_j}^1$, the Eq. A3 and Eq. A8 present the solution for the original Hardy's paradox with Hardy's value in Eq. A11 under the quantum state Eq. A1. This certifies the nonlocality through the original Hardy's paradox.

To accommodate the situation with imperfect detection, we assume that detectors in Alice and Bobs' laboratories are symmetric with efficiency η . When considering imperfect system detection efficiency η , we would like to claim that the zero Hardy conditions $P(00|A_2B_2) = 0$, $P(01|A_1B_2) = 0$, and $P(10|A_2B_1) = 0$ still hold. The difference is that there will occur undetected events u in both Alice and Bob's laboratories. Inspired by the Ref. [53], this situation can be analyzed with the help of the LHV model presented by Eberhard [52]. Based on the above analysis, the observable basis vectors are

$$\begin{aligned} |A_2^0\rangle &= \frac{1}{\sqrt{\cos(\theta) + \sin(\theta)}} (\sqrt{\sin(\theta)}|0\rangle + \sqrt{\cos(\theta)}|1\rangle), \\ |A_2^1\rangle &= \frac{1}{\sqrt{\cos(\theta) + \sin(\theta)}} (\sqrt{\cos(\theta)}|0\rangle - \sqrt{\sin(\theta)}|1\rangle), \end{aligned} \quad (\text{A12})$$

and

$$\begin{aligned} |B_2^0\rangle &= \frac{1}{\sqrt{\cos(\theta) + \sin(\theta)}} (-\sqrt{\cos(\theta)}|0\rangle + \sqrt{\sin(\theta)}|1\rangle), \\ |B_2^1\rangle &= \frac{1}{\sqrt{\cos(\theta) + \sin(\theta)}} (\sqrt{\sin(\theta)}|0\rangle + \sqrt{\cos(\theta)}|1\rangle), \end{aligned} \quad (\text{A13})$$

and

$$\begin{aligned} |A_1^0\rangle &= \frac{1}{\sqrt{\cos(\theta)^3 - \sin(\theta)^3}} (\sin(\theta)^{3/2}|0\rangle - \cos(\theta)^{3/2}|1\rangle), \\ |A_1^1\rangle &= \frac{1}{\sqrt{\cos(\theta)^3 - \sin(\theta)^3}} (\cos(\theta)^{3/2}|0\rangle + \sin(\theta)^{3/2}|1\rangle), \end{aligned} \quad (\text{A14})$$

and

$$\begin{aligned} |B_1^0\rangle &= \frac{1}{\sqrt{\cos(\theta)^3 - \sin(\theta)^3}} (\cos(\theta)^{3/2}|0\rangle + \sin(\theta)^{3/2}|1\rangle), \\ |B_1^1\rangle &= \frac{1}{\sqrt{\cos(\theta)^3 - \sin(\theta)^3}} (-\sin(\theta)^{3/2}|0\rangle + \cos(\theta)^{3/2}|1\rangle). \end{aligned} \quad (\text{A15})$$

In this case, the angles for Alice and Bob's measurements should be

$$\begin{aligned} \tan(\theta_{A_2}/2) &= \left(\frac{\cos(\theta)}{\sin(\theta)}\right)^{1/2}, \tan(\theta_{B_2}/2) = -\left(\frac{\sin(\theta)}{\cos(\theta)}\right)^{1/2}, \\ \tan(\theta_{A_1}/2) &= -\left(\frac{\cos(\theta)}{\sin(\theta)}\right)^{3/2}, \tan(\theta_{B_1}/2) = \left(\frac{\sin(\theta)}{\cos(\theta)}\right)^{3/2}, \end{aligned} \quad (\text{A16})$$

where e.g. $A_i = \cos(\theta_{A_i})\sigma_z + \sin(\theta_{A_i})\sigma_x = \Pi_{A_i}^0 - \Pi_{A_i}^1$ and $B_j = \cos(\theta_{B_j})\sigma_z + \sin(\theta_{B_j})\sigma_x = \Pi_{B_j}^0 - \Pi_{B_j}^1$. When the measurements for Alice and Bob are taken as above, the Hardy's conditions can be directly satisfied

$$P(00|A_2B_2) = 0, P(01|A_1B_2) = 0, P(10|A_2B_1) = 0. \quad (\text{A17})$$

Further by considering the effect of imperfect detection efficiency, one has,

$$\begin{aligned} |A_i^a\rangle &= \sqrt{\eta}|A_i'^a\rangle + \sqrt{1-\eta}|A_i'^{a,u}\rangle, \\ |B_j^b\rangle &= \sqrt{\eta}|B_j'^b\rangle + \sqrt{1-\eta}|B_j'^{b,u}\rangle, \end{aligned} \quad (\text{A18})$$

here, $|A_i'^{a,u}\rangle$ ($|B_j'^{b,u}\rangle$) are vectors corresponding with un-detected events and orthogonal to $|A_i'^a\rangle$ ($|B_j'^b\rangle$). Thus, there will be inconclusive events that should be taken into consideration in Hardy's test. According to the Ref. [53], the Eberhard inequality can be used to analyze the effect of non-perfect detection for experimental Hardy's test. Specifically, when Hardy's conditions are satisfied, the LHV model should satisfy the following constraints

$$P(00|A_1B_1) - P(0u|A_1B_2) - P(u0|A_2B_1) \leq 0. \quad (\text{A19})$$

From Eq. A10d, Eq. A10b, Eq. A10c and Eq. A18, we have

$$\begin{aligned} P(00|A_1B_1) &= \eta^2 \left[\frac{\cos(\theta)\sin(\theta)(\cos(\theta) - \sin(\theta))}{1 - \cos(\theta)\sin(\theta)} \right]^2, \\ P(0u|A_1B_2) &= \eta(1-\eta) \frac{[\cos(\theta)\sin(\theta)]^2}{1 - \cos(\theta)\sin(\theta)}, \\ P(u0|A_2B_1) &= \eta(1-\eta) \frac{[\cos(\theta)\sin(\theta)]^2}{1 - \cos(\theta)\sin(\theta)}. \end{aligned} \quad (\text{A20})$$

Defining the following function of θ and η ,

$$P_{\text{Hardy}}(\theta, \eta) = P(00|A_1B_1) - P(0u|A_1B_2) - P(u0|A_2B_1). \quad (\text{A21})$$

When the maximal violation of Hardy's paradox is achieved and considering $\theta \in [0, \frac{\pi}{2}]$, there should be

$$\frac{\partial P_{\text{Hardy}}(\theta, \eta)}{\partial \theta} = 0 \Rightarrow \theta = \frac{1}{2} \arcsin \left(3 - \sqrt{\frac{6\eta - 1}{2\eta - 1}} \right). \quad (\text{A22})$$

Recalling the Eq. A16, this gives the optimal quantum states and observables at given different detection efficiency η . The maximal violation at detection efficiency η is termed as

$$P_{\text{Hardy}}^{\max}(\eta) = \frac{1}{2} [1 - \sqrt{1 + 4\eta(3\eta - 2)}] + 3\eta [1 - 3\eta + \sqrt{1 + 4\eta(3\eta - 2)}]. \quad (\text{A23})$$

For the quantum state in the Eq. A1, there will be positive Hardy's values $P_{\text{Hardy}}^{\max} > 0$ only when $\eta > \frac{2}{3}$. In Table II, we present the optimal quantum states and observables together with maximal Hardy's values at detection efficiencies around $\eta = 82\%$.

η	θ_{A_1}	θ_{A_2}	θ_{B_1}	θ_{B_2}	θ	$P(00 A_2B_2)$	$P(01 A_1B_2)$	$P(10 A_2B_1)$	$P(00 A_1B_1)$	$P(0u A_1B_2)$	$P(u0 A_2B_1)$	$P_{\text{Hardy}}^{\max}(\eta)$
0.788	-2.90572	2.22849	0.235875	-0.913103	0.236716	0	0	0	0.029457	0.011246	0.011246	0.00696561
0.8	-2.88135	2.20203	0.260239	-0.939565	0.252261	0	0	0	0.033588	0.012326	0.012326	0.00893709
0.81	-2.86136	2.18172	0.280231	-0.959875	0.2646	0	0	0	0.037038	0.013117	0.013117	0.0108044
0.82	-2.84165	2.16277	0.29994	-0.97882	0.276432	0	0	0	0.040478	0.013798	0.013798	0.0128816
0.83	-2.82223	2.14503	0.319365	-0.996562	0.287797	0	0	0	0.043894	0.01436	0.01436	0.0151737
0.84	-2.80308	2.12835	0.338509	-1.01324	0.298732	0	0	0	0.047274	0.014794	0.014794	0.0176853
0.85	-2.78422	2.11262	0.357376	-1.02897	0.30927	0	0	0	0.050606	0.015093	0.015093	0.0204202

TABLE II. Optimal quantum states and measurement setting versus detection efficiency η . In the optimization, the detection efficiency for detectors in Alice and Bob's laboratories is assumed to be symmetric. The θ , θ_{A_i} and θ_{B_j} with $i, j \in 1, 2$ are parameters for the quantum state, Alice's measurement settings and Bob's measurement settings, respectively.

In the experiment, apart from detection efficiency, there exist other system parameters that influence the maximal violation of Hardy's paradox, among which the fidelity of the state and the average photon number per pulse are of utmost importance. We conducted simulations for these variables as well to guide our parameter selection in the experiment. The entangled photon pairs are prepared using an SPDC source, the pulses of which may include the vacuum and multiple pairs of photons besides single pair of photons. We assume that the probabilities for the component of n pairs of photons in the output of an SPDC source follow the Poisson distribution,

$$P(n) = \frac{\mu^n}{n!} e^{-\mu}, \quad (\text{A24})$$

where μ is the mean photon number in the output of the SPDC source. For each pair of photons, the experimentally prepared quantum state may be imperfect that could deviate from the one defined in Eq. A1. We use the Werner state to simulate the prepared state. Which can be written as:

$$\rho = V|\Psi(\theta)\rangle\langle\Psi(\theta)| + \frac{1-V}{4}I \quad (\text{A25})$$

where V is the visibility of the state, and the corresponding fidelity is $F = (3V + 1)/4$.

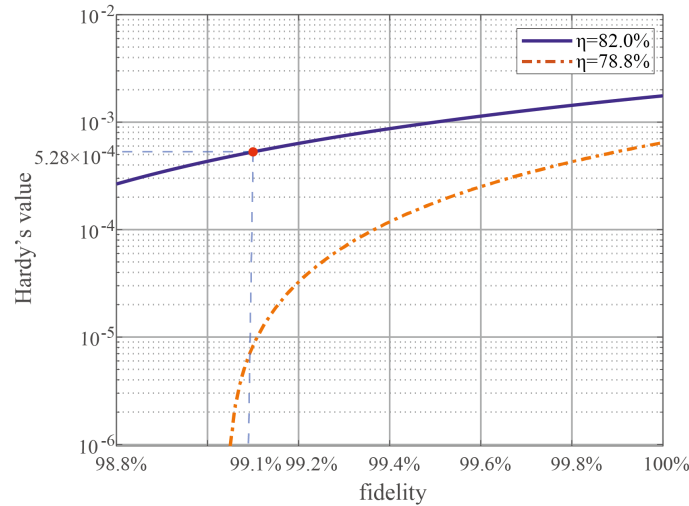


FIG. 4. Hardy's values versus fidelity for $\eta = 78.8\%$ and $\eta = 82\%$. The red point represent the Hardy's value of 5.28×10^{-4} for our system.

As shown in Fig. 4, we present the relations between Hardy's value and fidelity under detection efficiencies $\eta = 78.8\%$ and 82% . Here, $\eta = 82\%$ is the detection efficiency for parameter optimization in this work, which is slightly lower than the system detection efficiencies in our experiment. $\eta = 78.8\%$ is taken from Ref. [11], which is one of the latest loophole-free Bell inequality tests. From the results of Fig. 4, the theoretical Hardy's value should be less than 10^{-6} with the detection efficiency (78.88%) and fidelity (98.66%) in Ref. [11]. While, for our system, the detection efficiency is around 82% , and the fidelity is 99.10% . We can realise a Hardy's value of 5.28×10^{-4} theoretically (the red point in Fig. 4).

Appendix B: Experimental Details

1. Modeling the inconclusive events

Recalling the schematic setup in the main text, there are two threshold single photon detectors on Alice's (Bob's) side. The one on the transmission path after PBS corresponding to the result 0, and the other on the reflection path corresponding to 1. Because of the imperfect detection efficiency, dark counts, the vacuum state and multiple photon pairs in the output of SPDC source, there will be two kinds of inconclusive events that both two detectors on one side click or neither has a click. In this experiment, in order to close the *detection loophole*, we treat both inconclusive events as u .

2. Quantum state characterization

To obtain the maximal Hardy's values in our experiment, the quantum state is set to be the non-maximally polarization entangled two-photon state $\cos(0.2764)|HV\rangle + \sin(0.2764)|VH\rangle$ and we set the angles for single photon polarization state measurement to be $\theta_{A_1} = -2.8417, \theta_{A_2} = -2.1628$ for Alice, $\theta_{B_1} = 0.2999, \theta_{B_2} = -0.9788$ for Bob (i.e. the optimized quantum state and measurement settings for $\eta = 82\%$ in Sec. A). To create this quantum state in the experiment, we measure diagonal/anti-diagonal visibility in the bases set $(\pi/4, -0.2764), (\pi/2 + 0.2764, \pi/4)$ for minimum coincidence, and in the bases set $(\pi/4, \pi/2 - 0.2764), (0.2764, \pi/4)$ for maximum coincidence, where the angles represent measurement basis $\cos(\theta)\sigma_z + \sin(\theta)\sigma_x$ for Alice and Bob. Meanwhile, we perform the state tomography measurement on the non-maximally entangled state. We use the maximum likelihood estimation of density matrices to calculate the fidelity to avoid the problem of experimental inaccuracies and statistical fluctuations of coincidence counts.

We generate a formula for an explicitly "physical" density matrix, i.e., a matrix that has the three important properties of normalization, Hermiticity, and positivity. This matrix will be a function of 16 real variables with $t = \{t_1, t_2, \dots, t_{16}\}$ and is denoted as $\rho_p(t)$. For any matrix that can be written in the form $G = T^\dagger T$ must be non-negative definite. The explicitly "physical" density matrix ρ_p is given by the formula

$$\rho_p = T^\dagger(t)T(t)/\text{Tr}\{T^\dagger(t)T(t)\} \quad (\text{B1})$$

and it is convenient to choose a tridiagonal form for T :

$$T(t) = \begin{bmatrix} t_1 & 0 & 0 & 0 \\ t_5 + it_6 & t_2 & 0 & 0 \\ t_{11} + it_{12} & t_7 + it_8 & t_3 & 0 \\ t_{15} + it_{16} & t_{13} + it_{14} & t_9 + it_{10} & t_4 \end{bmatrix} \quad (\text{B2})$$

The measurement data consists of a set of coincidence counts n_μ whose expected value is $\bar{n}_\mu = N\langle\phi_\mu|\rho|\phi_\mu\rangle$. Here ρ is the prepared quantum state. In our experiment $\mu = 1, 2, \dots, 36$, $|\phi_\mu\rangle\langle\phi_\mu|$ is the operator of the projection measurement of the two-photon state, and for each photon we measured in the bases $|H\rangle, |V\rangle, |+\rangle, |-\rangle, |R\rangle, |L\rangle$, there are 36 projection measurements for ρ , $\phi_\mu \in |HH\rangle, |HV\rangle, \dots, |RL\rangle, |RR\rangle$. Assuming that the noise on these coincidence measurements has a Gaussian probability distribution. Thus the probability of obtaining a set of 36 counts n_1, n_2, \dots, n_{36} is

$$P(n_1, n_2, \dots, n_{36}) = \frac{1}{N_{\text{norm}}} \prod_{\mu=1}^{36} \exp\left[-\frac{(n_\mu - \bar{n}_\mu)^2}{2\sigma_\mu^2}\right] \quad (\text{B3})$$

where σ_μ is the standard deviation for the n -th coincidence measurement (given approximately by $\sqrt{\bar{n}_\mu}$) and N_{norm} is the normalization constant. For our physical density matrix ρ_p , the number of counts expected for the n -th measurement is

$$\bar{n}_\mu(t_1, t_2, \dots, t_{16}) = N\langle\phi_\mu|\rho_p(t_1, t_2, \dots, t_{16})|\phi_\mu\rangle \quad (\text{B4})$$

Thus the likelihood that the matrix $\rho_p(t_1, t_2, \dots, t_{16})$ could produce the measured data n_1, n_2, \dots, n_{36} is

$$P(n_1, n_2, \dots, n_{36}) = \frac{1}{N_{\text{norm}}} \prod_{\mu=1}^{36} \exp\left[-\frac{(N\langle\phi_\mu|\rho_p(t_1, t_2, \dots, t_{16})|\phi_\mu\rangle - n_\mu)^2}{2N\langle\phi_\mu|\rho_p(t_1, t_2, \dots, t_{16})|\phi_\mu\rangle}\right] \quad (\text{B5})$$

Rather than to find the maximum value of $P(t_1, t_2, \dots, t_{16})$, it simplifies things somewhat to find the maximum of its logarithm (which is mathematically equivalent). Thus the optimization problem reduces to finding the minimum of the following function:

$$L(t_1, t_2, \dots, t_{16}) = \sum_{\mu=1}^{36} \frac{(N\langle\phi_\mu|\rho_p(t_1, t_2, \dots, t_{16})|\phi_\mu\rangle - n_\mu)^2}{2N\langle\phi_\mu|\rho_p(t_1, t_2, \dots, t_{16})|\phi_\mu\rangle} \quad (\text{B6})$$

This is the “likelihood” function that we employed in our numerical optimization routine. The result is shown in Fig. 5, the state fidelity is 99.10%. The coordinate axis labeled by HH, HV, VH and VV for the density operator ρ can be written as:

$$\rho = \rho_{11}|HH\rangle\langle HH| + \rho_{12}|HH\rangle\langle HV| + \dots + \rho_{44}|VV\rangle\langle VV| \quad (B7)$$

where ρ_{ij} if the elements of the density operator matrix. The main imperfections are attributed to the multi-photon components, imperfect optical elements, and imperfect spatial/spectral mode matching.

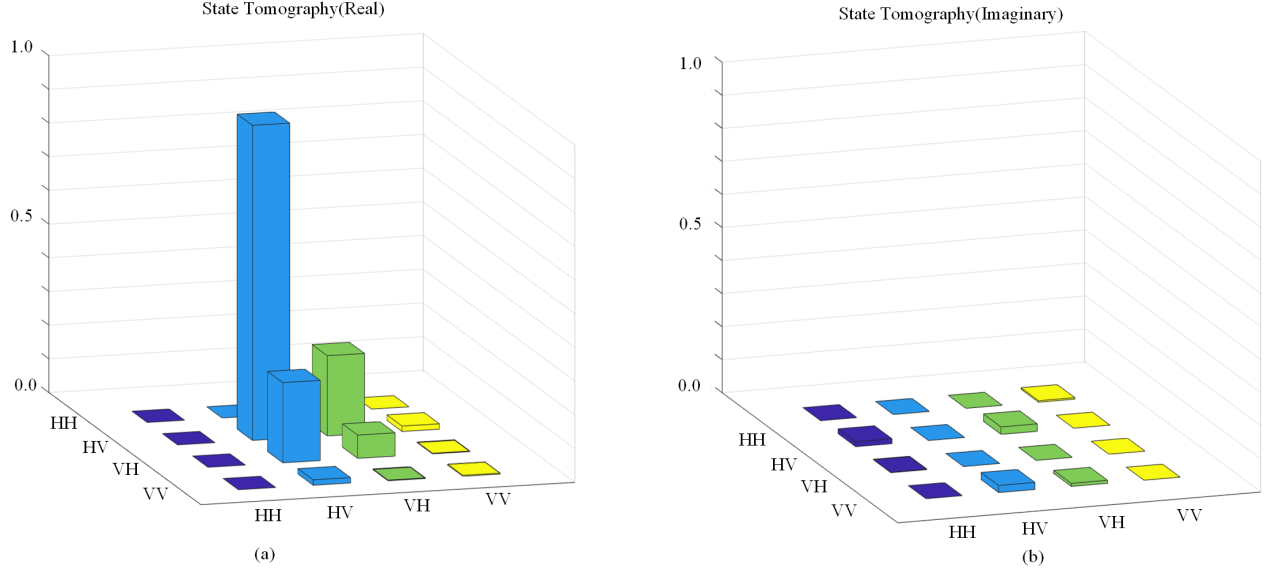


FIG. 5. (color online) Tomography of the prepared quantum state. The real and imaginary parts are shown in (a) and (b), respectively.

3. Spacetime configuration of the experiment

To rule out the locality loophole, space-like separation must be satisfied between measurement events at Alice and Bob’s measurement stations, i.e., the setting choice and measurement outcome at one station must be space-like separated from the events at the other station (see Fig. 6). Therefore, we then obtain

$$\begin{cases} (|SA| + |SB|)/c > T_E - (L_{SA} - L_{SB})/c + T_{QRNG1} + T_{Delay1} + T_{PC1} + T_{M2} \\ (|SA| + |SB|)/c > T_E + (L_{SA} - L_{SB})/c + T_{QRNG2} + T_{Delay2} + T_{PC2} + T_{M1} \end{cases} \quad (B8)$$

where $|SA| = 93$ m ($|SB| = 90$ m) is the free space distance between entanglement source and Alice’s (Bob’s) measurement station. $T_E = 10$ ns is the generation time for photon pairs, which is mainly contributed by the 10 ns pump pulse duration. $L_{SA} = 188$ m ($L_{SB} = 169$ m) is the effective optical path that is mainly contributed by the 129 m (116 m) long fiber between the source and Alice’s (Bob’s) measurement station. $T_{QRNG1} = T_{QRNG2} = 96$ ns is the time elapse for QRNG to generate a random bit. $T_{Delay1} = 270$ ns ($T_{Delay2} = 230$ ns) is the delay between the random numbers being generated and delivered to the Pockels cell. $T_{PC1} = 112$ ns ($T_{PC2} = 100$ ns) is the waiting time for the Pockels cell to be ready to perform state measurements after receiving the random numbers, including the internal delay of the Pockels Cells (62 ns, 50 ns) and the time for Pockels cell to stabilize before performing single photon polarization state projection after switching of 50 ns. $T_{M1} = 55$ ns ($T_{M2} = 100$ ns) is the time elapse for SNSPD to output an electronic signal, including the delay due to fiber and cable length (in our experiment, the fiber and cable used in Alice or Bob after the two coupler has the same length. The time difference caused by them is less than 2 ns, so we neglect it in analysis). The electronic signals generated by SNSPD are considered clonable and thus represent a definite classical entity. While the photon involved in the entangled state is considered unclonable according to quantum physics. Therefore, we can reasonably assume that the photons collapse upon reaching the SNSPD, thereby concluding the measurement of the photon at the SNSPD. In that sense, the collapse-locality loophole, which concerns where the measurement outcomes eventually arise in space-time, was strongly tighten.

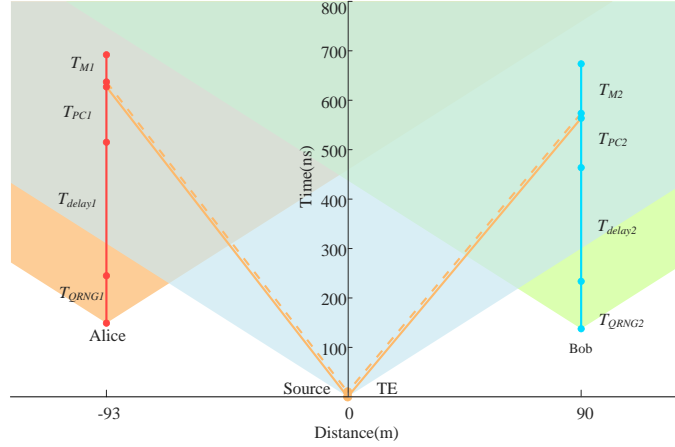


FIG. 6. Space-time diagram for the experimental events. $T_E = 10$ ns is the generation time of entangled photon pairs. $T_{QRNG1,2}$ are duration of times required to generate random bits to switch the Pockels cells. $T_{delay1,2}$ are the delay time between the random bits being generated and received by the Pockels cells. $T_{PC1,2}$ are the waiting times for the Pockels cells to perform state measurements after receiving the random bits. $T_{M1,2}$ are the times taken by the single photon detectors to output electronic signals. $T_{QRNG1} = T_{QRNG2} = 96$ ns, $T_{delay1} = 270$ ns, $T_{delay2} = 230$ ns, $T_{PC1} = 112$ ns, $T_{PC2} = 100$ ns, $T_{M1} = 55$ ns and $T_{M2} = 100$ ns. Alice's and Bob's measurement stations are placed on opposite sides of the source at distances of 93 m and 90 m, respectively. The effective optical length between Alice's (Bob's) station and the source is 132 m (119 m). This arrangement ensures no signalling between relevant events in the experiment. The shaded areas are the future light cones for the source, Alice's and Bob's laboratories.

Measurement independence between entangled-pair creation event and setting choice events is satisfied by the following spacelike separation configuration:

$$\begin{cases} |SA|/c > L_{SA}/c - T_{Delay1} - T_{PC1}, \\ |SB|/c > L_{SB}/c - T_{Delay2} - T_{PC2}. \end{cases} \quad (B9)$$

We estimate the fiber length by measuring the reflection, the single photon arrives at the SNSPD and generates an electronic response with high efficiency. However, with a small possibility, the photon is reflected by the SNSPD chip, travels to the source, gets polarization rotated in the Sagnac loop, and then travels back to SNSPD, making the second click. We measure the electronic cable length using a ruler. By subtracting the time for the signal passing through the fiber and cable, as well as the delay caused by the discriminator, we estimate the effective fiber length between the Pockels cell and the SNSPD chip. The measured fiber length, cable length, and discriminating time are summarized in Tab. III.

TABLE III. The fiber distances between Source and Measurement.

	Source-PC	PC-SNSPD	SNSPD-TDC
Alice	129 m	11 m	4 m
Bob	116 m	20 m	12 m

4. Determination of single photon efficiency

We use the heralding efficiency as the single photon efficiency in our experiment. The heralding efficiency is defined as $\eta_A = C/N_B$ and $\eta_B = C/N_A$ for Alice and Bob, Where C is the coincidence events and N_A, N_B is the single events for Alice and Bob measured in the experiment. The heralding efficiency is given by

$$\eta = \eta_{sc} \times \eta_{so} \times \eta_{fiber} \times \eta_m \times \eta_{det} \quad (B10)$$

where η_{sc} is the efficiency to couple entangled photons into single mode optical fiber, η_{so} is the efficiency for photons passing through the optical elements in the source, η_{fiber} is the transmittance of fiber connecting source to measurement station, η_m is the efficiency for light passing through the measurement station, and η_{det} is the single photon detector efficiency. We list the heralding efficiencies from the entangled photon source to detection stations, the transmission efficiencies of each intermediate process, and the detection efficiencies of the detectors in Tab. V. We measure the transmission efficiencies of each process and the detection efficiencies with classical light beams and NIST-traceable power metres,

TABLE IV. The efficiencies of optical elements.

Optical element	Efficiency
Aspherical lens	99.27% \pm 0.03%
Spherical lens	99.6% \pm 1.0%
Half wave plate (780 nm/1560 nm)	99.93% \pm 0.02%
Half wave plate (1560 nm)	99.92% \pm 0.04%
Quarter wave plate (1560 nm)	99.99% \pm 0.08%
Polarizing beam splitter (780 nm/1560 nm)	99.6% \pm 0.1%
Polarizing beam splitter (1560 nm)	99.6% \pm 0.2%
Dichoric mirror	99.46% \pm 0.03%
PPKTP	99.6% \pm 0.2%
Pockels cell	98.7% \pm 0.5%

TABLE V. Photon transmission and detection efficiencies in the experiment.

Parties	η	η_{sc}	η_{so}	η_{fiber}	η_m	η_{det}
Alice1	82.1%	94.3%	95.9%	99%	95.5%	96.0%
Alice2	82.4%				95.6%	96.3%
Bob1	82.1%	94.0%			95.2%	96.7%
Bob2	82.2%				95.5%	96.5%

Appendix C: Experimental results

1. Test of local realism

To convincingly quantify the results of the experiment, we perform a hypothesis test of local realism. The null hypothesis is that the experimental results can be explained by local realism. We use the p value obtained from test statistics to denote the maximum probability that the observed experimental results can be obtained from local realism. Hence, we have to show that our results correspond to a very small p value so that they can indicate a strong rejection of local hidden-variable models. We apply the prediction-based radio (PBR) method to design the test statistics and compute the upper bound of the p value.

Denote Alice's and Bob's random settings distribution at each trial as $p_A(x)$ and $p_B(y)$ where $x, y \in \{0, 1\}$. We assume the joint probability distribution of them p_{xy} is fixed and known before running the test. The measurement outcomes of Alice and Bob at each trial are denoted by A and B with possible value $a, b \in \{0, 1, u\}$. In practice, we can only obtain the frequency of different outcomes $\mathbf{f} \equiv \{n(abxy)/N, a, b = 0, 1, u; x, y = 0, 1\}$, where n is number of trials the result (a, b, x, y) appears and N is the number of the total experimental trials. So, at the beginning of the test, we have to use the maximum likelihood method to find out the no-signaling distribution $\mathbf{P}_{NS}^* \equiv \{p_{xy}p_{NS}^*(ab|xy), a, b = 0, 1, u; x, y = 0, 1\}$ that has the minimum distance from the observed frequency distribution \mathbf{f} . When the trials is large enough, \mathbf{P}_{NS}^* can be close to the true probability distribution.

Particularly, we use the Kullback-Leribler (KL) Ref. [56] divergence to measure this distance because it's the optimal asymptotic efficiency for rejecting the null hypothesis.

$$D_{KL}(\mathbf{f}||\mathbf{P}_{NS}) = \sum_{a,b,x,y} p_{xy} f(ab|xy) \log_2 \left(\frac{f(ab|xy)}{p_{NS}(ab|xy)} \right). \quad (C1)$$

Hence, the optimal no-signaling distribution \mathbf{P}_{NS}^* is the solution of the optimization

$$\min_{\mathbf{P}_{NS} \in \mathcal{P}_{NS}} D_{KL}(\mathbf{f}||\mathbf{P}_{NS}). \quad (C2)$$

After this estimation, we can find the optimal local realistic distribution \mathbf{P}_{LR}^* that has the minimum distance from our nearly true probability distribution.

$$\mathbf{P}_{LR}^* = \arg \min_{\mathbf{P}_{LR} \in \mathcal{P}_{LR}} D_{KL}(\mathbf{P}_{NS}^*||\mathbf{P}_{LR}) = \sum_{a,b,x,y} p_{xy} p_{NS}^*(ab|xy) \log_2 \left(\frac{p_{NS}^*(ab|xy)}{p_{LR}(ab|xy)} \right). \quad (C3)$$

According to Ref. [51] after k trials but before the $(k+1)$ -st trial the PBR protocol returns a special Bell inequality of the form

$$\langle R_k(x) \rangle \leq 1 \quad (C4)$$

with $R_k(x)$ nonnegative. Any such sequence of inequalities can be seen as a prediction-based radio (PBR) yielding a valid p value computed according to

$$p^{(PBR)} = \min \left(\left(\prod_{i=1}^n R_{k-1}(x_k) \right)^{-1}, 1 \right) \quad (C5)$$

The proof can be found in Ref. [51] Sec.III C.

Once the optimal local realistic distribution \mathbf{P}_{LR}^* is found, with the local realistic distribution constraint according to Ref. [51]

$$\sum_{a,b,x,y} \frac{p_{NS}^*(ab|xy)}{p_{LR}^*(ab|xy)} p_{xy} p_{LR}(ab|xy) \leq 1 \quad (C6)$$

The test statistics $R(ABXY) \equiv \frac{p_{NS}^*(ab|xy)}{p_{LR}^*(ab|xy)}$ can be seen as PBR to perform a hypothesis test of local realism. To avoid the i.i.d. (independent and identical distribution) assumption in the test, one needs to construct the test statistics $R_i(A_i B_i X_i Y_i)$ for the i -th trial before it's practical outcome, that's why this method named prediction-based radio method. To realize this prediction, we divide the total data into 2.4×10^7 trial sized block. For the first data block, we set $R(ABXY) = 1$. For the following block i we construct the $R_i(A_i B_i X_i Y_i)$ based on the frequency distribution of the $i - 1$ block. With the PBRs constructed, the p value upper bound of the n trials for rejecting local realism is given by:

$$p_n = \min \left(\left(\prod_{i=1}^n R_i(A_i B_i X_i Y_i) \right)^{-1}, 1 \right) \quad (C7)$$

where $a_i b_i$ and $x_i y_i$ are the measurement outcomes and setting choices at the i -th trial. The results observed in 6 hours with $n = 5.32 \times 10^9$ show that the p value for obtaining our result by the local realism is upper bounded by 10^{-16348} . This shows an extremely strong evidence against local realism provided by our experiment output.

2. Test of no signaling

We checked whether our experimental data are in agreement with the no-signaling principle by a traditional hypothesis test with the i.i.d. assumption. In the experiment, there are eight no-signaling conditions: Alice obtains 0 or 1 under the setting $x = 0$ or 1 is independent of Bob's setting choice, and Bob obtains 0 or 1 under the setting $y = 0$ or 1 is independent of Alice's setting choice. We don't mention the situation that Alice(Bob)'s outcomes u because if Alice(Bob) obtains o and e independently, then we can deduce that she(he) can outcome u freely, too. We construct the test statistics of no-signaling with the method named two-proportion Z-test. This method is always used to determine whether two samples are drawn from the same population. Generally, if the p-value is larger than 0.05 we can say no evidence of violating the no-signaling principle by our experimental data. The p-value that we found is in the following table:

TABLE VI. p values for the hypothesis test of no-signalling

p value input	output		
		out = 1	out = 0
$x = 0$		0.3948	0.7823
$x = 1$		0.7482	0.7729
$y = 0$		0.4667	0.3560
$y = 1$		0.0604	0.9518

-
- [1] A. Einstein, B. Podolsky, and N. Rosen, Can quantum-mechanical description of physical reality be considered complete?, *Phys. Rev.* **47**, 777 (1935).
 - [2] D. Bohm, A suggested interpretation of the quantum theory in terms of "hidden" variables. I, *Phys. Rev.* **85**, 166 (1952).
 - [3] J. S. Bell, On the einstein podolsky rosen paradox, *Physics* **1**, 195 (1964).
 - [4] J. F. Clauser, M. A. Horne, A. Shimony, and R. A. Holt, Proposed experiment to test local hidden-variable theories, *Phys. Rev. Lett.* **23**, 880 (1969).

- [5] N. Brunner, D. Cavalcanti, S. Pironio, V. Scarani, and S. Wehner, Bell nonlocality, *Rev. Mod. Phys.* **86**, 419 (2014).
- [6] S. J. Freedman and J. F. Clauser, Experimental test of local hidden-variable theories, *Phys. Rev. Lett.* **28**, 938 (1972).
- [7] A. Aspect, P. Grangier, and G. Roger, Experimental realization of einstein-podolsky-rosen-bohm gedankenexperiment: A new violation of bell's inequalities, *Phys. Rev. Lett.* **49**, 91 (1982).
- [8] B. Hensen, H. Bernien, A. E. Dréau, A. Reiserer, N. Kalb, M. S. Blok, J. Ruitenberg, R. F. Vermeulen, R. N. Schouten, C. Abellán, *et al.*, Loophole-free Bell inequality violation using electron spins separated by 1.3 kilometres, *Nature* **526**, 682 (2015).
- [9] L. K. Shalm, E. Meyer-Scott, B. G. Christensen, P. Bierhorst, M. A. Wayne, M. J. Stevens, T. Gerrits, S. Glancy, D. R. Hamel, M. S. Allman, *et al.*, Strong loophole-free test of local realism, *Phys. Rev. Lett.* **115**, 250402 (2015).
- [10] M. Giustina, M. A. M. Versteegh, S. Wengerowsky, J. Handsteiner, A. Hochrainer, K. Phelan, F. Steinlechner, J. Kofler, J.-A. Larsson, C. Abellán, *et al.*, Significant-loophole-free test of Bell's theorem with entangled photons, *Phys. Rev. Lett.* **115**, 250401 (2015).
- [11] M.-H. Li, C. Wu, Y. Zhang, W.-Z. Liu, B. Bai, Y. Liu, W. Zhang, Q. Zhao, H. Li, Z. Wang, *et al.*, Test of local realism into the past without detection and locality loopholes, *Phys. Rev. Lett.* **121**, 080404 (2018).
- [12] D. Rauch, J. Handsteiner, A. Hochrainer, J. Gallicchio, A. S. Friedman, C. Leung, B. Liu, L. Bulla, S. Ecker, F. Steinlechner, *et al.*, Cosmic bell test using random measurement settings from high-redshift quasars, *Phys. Rev. Lett.* **121**, 080403 (2018).
- [13] S. Storz, J. Schär, A. Kulikov, P. Magnard, P. Kurpiers, J. Lütolf, T. Walter, A. Copetudo, K. Reuer, A. Akin, *et al.*, Loophole-free bell inequality violation with superconducting circuits, *Nature* **617**, 265 (2023).
- [14] D. Mayers and A. Yao, Quantum cryptography with imperfect apparatus, in *Proceedings 39th Annual Symposium on Foundations of Computer Science (Cat. No. 98CB36280)* (IEEE, 1998) pp. 503–509.
- [15] J. Barrett, L. Hardy, and A. Kent, No signaling and quantum key distribution, *Phys. Rev. Lett.* **95**, 010503 (2005).
- [16] A. Acín, N. Gisin, and L. Masanes, From bell's theorem to secure quantum key distribution, *Phys. Rev. Lett.* **97**, 120405 (2006).
- [17] A. Acín, N. Brunner, N. Gisin, S. Massar, S. Pironio, and V. Scarani, Device-independent security of quantum cryptography against collective attacks, *Phys. Rev. Lett.* **98**, 230501 (2007).
- [18] R. Colbeck, Quantum and relativistic protocols for secure multi-party computation, *Ph.D. thesis, Univ. of Cambridge* (2007).
- [19] S. Pironio, A. Acín, S. Massar, A. B. de La Giroday, D. N. Matsukevich, P. Maunz, S. Olmschenk, D. Hayes, L. Luo, T. A. Manning, *et al.*, Random numbers certified by bell's theorem, *Nature* **464**, 1021 (2010).
- [20] R. Colbeck and R. Renner, Free randomness can be amplified, *Nat. Phys.* **8**, 450 (2012).
- [21] P. Bierhorst, E. Knill, S. Glancy, Y. Zhang, A. Mink, S. Jordan, A. Rommal, Y.-K. Liu, B. Christensen, S. W. Nam, *et al.*, Experimentally generated randomness certified by the impossibility of superluminal signals, *Nature* **556**, 223 (2018).
- [22] Y. Liu, Q. Zhao, M.-H. Li, J.-Y. Guan, Y. Zhang, B. Bai, W. Zhang, W.-Z. Liu, C. Wu, X. Yuan, *et al.*, Device-independent quantum random-number generation, *Nature* **562**, 548 (2018).
- [23] Y. Zhang, L. K. Shalm, J. C. Bienfang, M. J. Stevens, M. D. Mazurek, S. W. Nam, C. Abellán, W. Amaya, M. W. Mitchell, H. Fu, *et al.*, Experimental low-latency device-independent quantum randomness, *Phys. Rev. Lett.* **124**, 010505 (2020).
- [24] L. K. Shalm, Y. Zhang, J. C. Bienfang, C. Schlager, M. J. Stevens, M. D. Mazurek, C. Abellán, W. Amaya, M. W. Mitchell, M. A. Alhejji, *et al.*, Device-independent randomness expansion with entangled photons, *Nat. Phys.* **17**, 452 (2021).
- [25] M.-H. Li, X. Zhang, W.-Z. Liu, S.-R. Zhao, B. Bai, Y. Liu, Q. Zhao, Y. Peng, J. Zhang, Y. Zhang, *et al.*, Experimental realization of device-independent quantum randomness expansion, *Phys. Rev. Lett.* **126**, 050503 (2021).
- [26] W.-Z. Liu, Y.-Z. Zhang, Y.-Z. Zhen, M.-H. Li, Y. Liu, J. Fan, F. Xu, Q. Zhang, and J.-W. Pan, Toward a photonic demonstration of device-independent quantum key distribution, *Phys. Rev. Lett.* **129**, 050502 (2022).
- [27] F. Xu, Y.-Z. Zhang, Q. Zhang, and J.-W. Pan, Device-independent quantum key distribution with random postselection, *Phys. Rev. Lett.* **128**, 110506 (2022).
- [28] D. P. Nadlinger, P. Dmota, B. C. Nichol, G. Araneda, D. Main, R. Srinivas, D. M. Lucas, C. J. Ballance, K. Ivanov, E.-Z. Tan, *et al.*, Experimental quantum key distribution certified by Bell's theorem, *Nature* **607**, 682 (2022).
- [29] W. Zhang, T. van Leent, K. Redeker, R. Garthoff, R. Schwonnek, F. Fertig, S. Eppelt, W. Rosenfeld, V. Scarani, C. C.-W. Lim, *et al.*, A device-independent quantum key distribution system for distant users, *Nature* **607**, 687 (2022).
- [30] C.-L. Li, K.-Y. Zhang, X. Zhang, K.-X. Yang, Y. Han, S.-Y. Cheng, H. Cui, W.-Z. Liu, M.-H. Li, Y. Liu, *et al.*, Device-independent quantum randomness-enhanced zero-knowledge proof, *Proc. Natl. Acad. Sci.* **120**, e2205463120 (2023).
- [31] V. Zapatero, T. van Leent, R. Arnon-Friedman, W.-Z. Liu, Q. Zhang, H. Weinfurter, and M. Curty, Advances in device-independent quantum key distribution, *npj Quantum Inf.* **9**, 10 (2023).
- [32] I. Šupić, J. Bowles, M.-O. Renou, A. Acín, and M. J. Hoban, Quantum networks self-test all entangled states, *Nat. Phys.* **19**, 670 (2023).
- [33] D. M. Greenberger, M. A. Horne, and A. Zeilinger, Going Beyond Bell's Theorem, in *Bell's Theorem, Quantum Theory and Conceptions of the Universe*, edited by M. Kafatos (Springer Netherlands, Dordrecht, 1989) pp. 69–72.
- [34] D. M. Greenberger, M. A. Horne, A. Shimony, and A. Zeilinger, Bell's theorem without inequalities, *Am. J. Phys.* **58**, 1131 (1990).
- [35] L. Hardy, Nonlocality for two particles without inequalities for almost all entangled states, *Phys. Rev. Lett.* **71**, 1665 (1993).
- [36] N. D. Mermin, Quantum mysteries refined, *Am. J. Phys.* **62**, 880 (1994).
- [37] A. Mukherjee, A. Roy, S. S. Bhattacharya, S. Das, M. R. Gazi, and M. Banik, Hardy's test as a device-independent dimension witness, *Phys. Rev. A* **92**, 022302 (2015).
- [38] H.-W. Li, M. Pawłowski, R. Rahaman, G.-C. Guo, and Z.-F. Han, Device- and semi-device-independent random numbers based on noninequality paradox, *Phys. Rev. A* **92**, 022327 (2015).
- [39] R. Rahaman, M. G. Parker, P. Mironowicz, and M. Pawłowski, Device-independent quantum key distribution based on measurement inputs, *Phys. Rev. A* **92**, 062304 (2015).
- [40] R. Ramanathan, M. Horodecki, H. Anwer, S. Pironio, K. Horodecki, M. Grünfeld, S. Muhammad, M. Bourennane, and P. Horodecki, Practical No-Signalling proof Randomness Amplification using Hardy paradoxes and its experimental implementation, arXiv preprint arXiv:1810.11648 (2018).
- [41] A. Rai, M. Pivoluska, S. Sasmal, M. Banik, S. Ghosh, and M. Plesch, Self-testing quantum states via nonmaximal violation in Hardy's

- test of nonlocality, [Phys. Rev. A **105**, 052227 \(2022\)](#).
- [42] S. Zhao, R. Ramanathan, Y. Liu, and P. Horodecki, Tilted hardy paradoxes for device-independent randomness extraction, [Quantum **7**, 1114 \(2023\)](#).
 - [43] D. Boschi, S. Branca, F. De Martini, and L. Hardy, Ladder proof of nonlocality without inequalities: Theoretical and experimental results, [Phys. Rev. Lett. **79**, 2755 \(1997\)](#).
 - [44] M. Barbieri, F. De Martini, G. Di Nepi, and P. Mataloni, Towards a test of non-locality without “supplementary assumptions”, [Phys. Lett. A **334**, 23 \(2005\)](#).
 - [45] G. Vallone, I. Gianani, E. B. Inostroza, C. Saavedra, G. Lima, A. Cabello, and P. Mataloni, Testing Hardy’s nonlocality proof with genuine energy-time entanglement, [Phys. Rev. A **83**, 042105 \(2011\)](#).
 - [46] L. Chen and J. Romero, Hardy’s nonlocality proof using twisted photons, [Opt. Express **20**, 21687 \(2012\)](#).
 - [47] E. Karimi, F. Cardano, M. Maffei, C. de Lisio, L. Marrucci, R. W. Boyd, and E. Santamato, Hardy’s paradox tested in the spin-orbit hilbert space of single photons, [Phys. Rev. A **89**, 032122 \(2014\)](#).
 - [48] L. Chen, W. Zhang, Z. Wu, J. Wang, R. Fickler, and E. Karimi, Experimental ladder proof of Hardy’s nonlocality for high-dimensional quantum systems, [Phys. Rev. A **96**, 022115 \(2017\)](#).
 - [49] M. Yang, H.-X. Meng, J. Zhou, Z.-P. Xu, Y. Xiao, K. Sun, J.-L. Chen, J.-S. Xu, C.-F. Li, and G.-C. Guo, Stronger Hardy-type paradox based on the Bell inequality and its experimental test, [Phys. Rev. A **99**, 032103 \(2019\)](#).
 - [50] S. Das and G. Paul, A new error-modeling of Hardy’s Paradox for superconducting qubits and its experimental verification, [ACM Trans. Quantum Comput. **1**, 1 \(2020\)](#).
 - [51] Y. Zhang, S. Glancy, and E. Knill, Asymptotically optimal data analysis for rejecting local realism, [Phys. Rev. A **84**, 062118 \(2011\)](#).
 - [52] P. H. Eberhard, Background level and counter efficiencies required for a loophole-free Einstein-Podolsky-Rosen experiment, [Phys. Rev. A **47**, R747 \(1993\)](#).
 - [53] W. Y. Hwang, I. G. Koh, and Y. D. Han, The detection loophole in hardy’s nonlocality theorem and minimum detection efficiency, [Phys. Lett. A **212**, 309 \(1996\)](#).
 - [54] G. Ghirardi and L. Marinatto, Hardy’s proof of nonlocality in the presence of noise, [Phys. Rev. A **74**, 062107 \(2006\)](#).
 - [55] D. Braun and M.-S. Choi, Hardy’s test versus the Clauser-Horne-Shimony-Holt test of quantum nonlocality: Fundamental and practical aspects, [Phys. Rev. A **78**, 032114 \(2008\)](#).
 - [56] S. Kullback and R. A. Leibler, On information and sufficiency, [Ann. Math. Stat. **22**, 79 \(1951\)](#).